FULL PAPER

Active, Programmable Elastomeric Surfaces with Tunable Adhesion for Deterministic Assembly by Transfer Printing

Andrew Carlson, Shuodao Wang, Paulius Elvikis, Placid M. Ferreira, Yonggang Huang, and John A. Rogers**

Active, programmable control of interfacial adhesion is an important, desired feature of many existing and envisioned systems, including medical tapes, releasable joints, and stamps for transfer printing. Here a design for an elastomeric surface that offers switchable adhesion strength through a combination of peel-rate dependent effects and actuation of sub-surface fluid chambers is presented. Microchannels and open reservoirs positioned under a thin surface membrane can be pressurized in a controlled manner to induce various levels of surface deformation via inflation. These pressurized structures demonstrate utility in controllably decreasing the strength of adhesion of flat, solid objects to the elastomeric surface, particularly in the limit of low peel-rates. Experimental and theoretical studies of these systems reveal the key mechanisms, and guide optimized geometries for broad control over adhesion, in a programmable and reversible manner. Implementing these concepts in stamps for transfer printing enables new modes for deterministic assembly of micro- and nanoscale materials onto diverse types of substrates. Collections of silicon plates delivered onto plastic, paper and other surfaces with single or multiply addressable stamps illustrate some of the capabilities.

1. Introduction

Assembly techniques based on transfer printing have become increasingly popular in the past several years, due to their unique capabilities in integration, assembly and fabrication of micro/nanomaterials.[1–16] Central to these techniques are strategies that facilitate the transfer of materials (i.e., inks, ranging from semiconductor nanostructures,[4,17–20] functional polymers,[21–23] organic molecular materials[24–27] and others[9,28,29]) in useful two or three dimensional layouts, onto substrates of interest. The most general form of this process utilizes a soft, elastomeric element (i.e., a stamp) to mediate physical mass transfer between a host or donor wafer and a secondary, receiving substrate. In many cases, thin adhesive layers or surface chemical modifications of the critical interfaces ensure efficient transfer.[30–32] A versatile alternative exploits rate-dependent viscoelastic effects to modulate adhesion to the stamp through peeling velocity. In this adhesiveless mode, the velocity of separation of the stamp from a surface influences the adhesive strength, with higher velocities yielding proportionally larger adhesion.[33,34] Here, material retrieval and delivery during printing occurs at high (≈10 cm/s or greater) or low (<1 mm/s) velocities, respectively, using a single stamp element. A growing number of applications in micro and nanotechnology benefit from or are enabled by printing-based assembly of this type, particularly in systems requiring heterogeneous integration of inorganic semiconductor materials into functional arrangements on plastic or rubber substrates. Examples include selective manipulation or massively parallel assembly of diverse collections of materials (i.e., Si,[2,19,35] GaN,[36] GaAs,[3,37,38] mica,[33] silica,[33] etc.) with various structural forms and sizes (nanometers to macroscopic dimensions), to yield high performance electronic and optoelectronic systems.

Efficient transfer relies critically on switching between strong (i.e., inking) and weak (i.e., printing) adhesion states in a rapid, robust, and repeatable manner. Of particular importance is achieving suitably weak adhesion to the stamp element during the delivery step. Kinetic approaches to decreasing adhesion are useful, but the minimum adhesion states are often larger than desired, thereby limiting the utility of transfer printing for certain cases. Recent efforts demonstrate strategies that can complement, or be used in conjunction with, those based on rate. In one example, targeted shear loading can facilitate interface fracture between a stamp and an ink, to enhance efficiency in release.[39] In another, switchability occurs through controlled sagging and retraction of a structured surface that

A. Carlson, Prof. J. A. Rogers
Department of Materials Science and Engineering
Fredrick Seitz Materials Research Laboratory
Beckman Institute for Advanced Science and Technology
University of Illinois at Urbana-Champaign
Urbana, IL, USA
E-mail: jrogers@illinois.edu
S. Wang, Prof. Y. Huang
Department of Civil and Environmental Engineering
Department of Mechanical Engineering
Northwestern University
Evanston, IL, USA
E-mail: y-huang@northwestern.edu
P. Elvikis, Prof. P. M. Ferreira
Department of Mechanical Sciences and Engineering
University of Illinois at Urbana-Champaign
Urbana, IL, USA

DOI: 10.1002/adfm.201201023

© 2012 WILEY-VCH Verlag GmbH & Co. KGaA, Weinheim

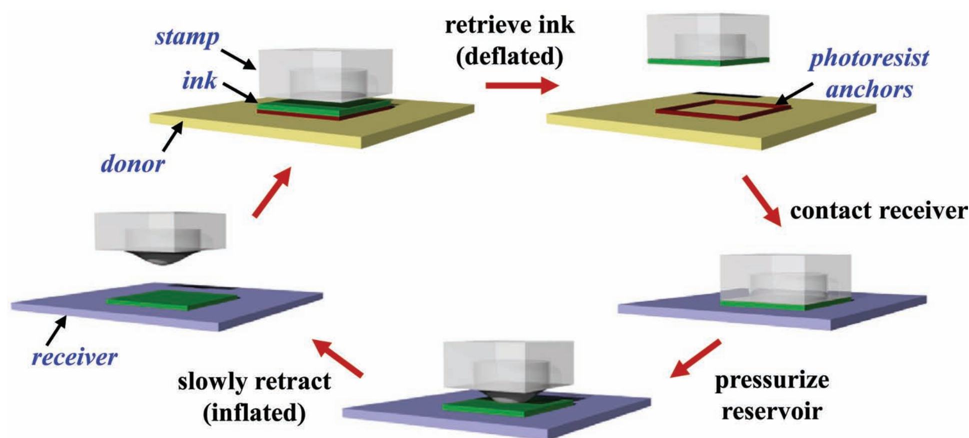

Figure 1. Procedure for printing with an elastomeric element that has a programmable surface shape for controlled adhesion, i.e., an active stamp. Initially the stamp, in a deflated state, is brought into contact with a rigid plate (i.e., ink) supported on a donor substrate. Rapid retraction retrieves the plate onto the stamp surface. The stamp, "inked" in this manner, is then lightly contacted to a receiver substrate. Pressurizing the reservoirs causes local inflation in the vicinity of the ink while slow retraction of the stamp releases the ink onto the receiver substrate.

supports pyramidal microtips.[40] Here, we report a protocol, shown in **Figure 1**, that reproduces the adhesion and release strategies of an aphid *pulvillus* in which localized regions of a microstructured elastomeric stamp are inflated/deflated in a fashion analagous to that of a balloon.[41] This construct yields continuously tunable and reversible levels of nonspecific, generalized adhesion. Mechanisms revealed by theoretical and experimental studies provide insights into the operation. We demonstrate these concepts in printing-based assembly of silicon plates onto a variety of substrates and configurations not easily accessible with other methods. To illustrate the versatility of this type of stamp and the feasibility of scaling it for use in massively parallel printing modes, we develop multiple independently-addressable and interconnected microstructured surfaces, capable of programmable operation. Silicon plates printed in a variety of orientations, geometries, and densities provide examples of some possibilities.

2. Actuated Elastomeric Stamps with Microchannels and Reservoirs

2.1. Microreservoir Stamp Design and Adhesiveless Transfer Printing Protocol

Figure 1 shows a schematic illustration of the transfer printing procedure. Here, the stamp has circular reservoirs embedded under its contacting surface, each of which can be inflated locally as a means of dynamically altering interfacial contact, and corresponding adhesive forces. For the retrieval step, the stamp surface is brought into intimate contact with the object to be transferred (green plate in Figure 1), positioned in co-centered alignment above a reservoir. Rapid retraction of the stamp in the deflated state (i.e., flat contacting surface) retrieves the plate, with an adhesion strength that is maximized by viscoelastic effects and complete areal interfacial contact.[40,42] The stamp, inked in this way, is then brought into contact with a receiving substrate (lavender surface in Figure 1). Pressurizing the reservoir causes the stamp surface to bulge around the interface. Upon slow retraction, the membrane inflates and peels continuously out of contact with the ink, starting at the outer perimeter and propagating toward the center. The equilibrium shape of the inflated membrane at any given stage of this process is defined by a complex interaction of reservoir pressure and contact area with the ink surface. As the retraction proceeds, however, the surface assumes an increasingly hemispherical geometry, thereby decreasing contact with the plate, ultimately to a central point, after which separation is completed.

Active stamps incorporate three critical components: 1) reservoirs embedded in raised features of relief on the surface, 2) narrow channels connecting these reservoirs to an external pressurization source (e.g., compressed gas), and 3) a thin (≈30 μm) membrane that covers the reservoirs and channels, and serves as the tunable interface between the stamp and ink. Such structures can be fabricated using techniques adapted from the microfluidics community.[43–46] **Figure 2**a provides a scanning electron microscope (SEM) image of a representative stamp of this type, created using soft lithographic methods from the elastomer polydimethylsiloxane (PDMS, Dow Corning Sylgard 184). This design incorporates a circular reservoir (225 μm in diameter and 70 μm in depth) and narrow channels (50 μm in width) embedded in a rectangular support. A membrane layer, composed of low modulus formulation of PDMS, completely covers the microstructured regions and is chemically bonded to the support post of Figure 2a, in a way that leaves it freely suspended across the reservoir and channels. An external pressure source connects to channel outlets at the perimeter of the structure (overall dimensions ≈10 mm × 10 mm). Pressurizing the reservoir with N_2 inflates the membrane;[47] Figure 2b,c show optical images of inflation under ≈12 psi pressure without and with a thin silicon platelet (250 μm × 250 μm × 3 μm) on its surface, respectively. Figure 2d provides an estimate of the

© 2012 WILEY-VCH Verlag GmbH & Co. KGaA, Weinheim

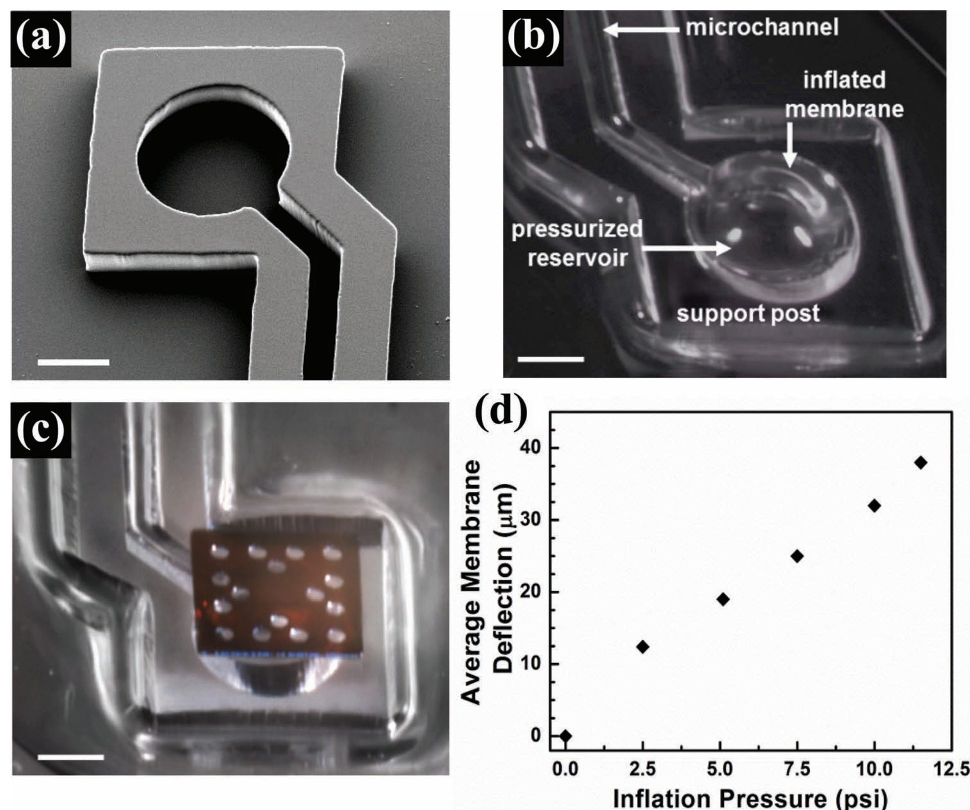

Figure 2. a) SEM image (20° tilt angle) of an active stamp without the top thin PDMS capping membrane. The microchannel leads directly from a remote gas inlet (not pictured) to a circular central reservoir embedded in the support post. Optical microscope images of an actuated stamp b) without and c) with a silicon plate on the inflated membrane; critical features are labeled. During inflation, the plate is pushed out of contact with the support post region of the stamp and remains connected only to a small central region of the inflated membrane. Here, the image consists of a compilation of images collected at different focal positions in a scanning stereomicroscope. d) Average deflection of the membrane during inflation, measured at the central point of the reservoir. Scale bars correspond to 100 μm.

membrane curvature at the center of the circular reservoir, obtained by using inflated stamps to mold features in low viscosity photocurable polyurethane and then performing surface profilometry on the molded surfaces. As expected, the points of maximum membrane deflection from the surface of the support post (flat, deflated state) increase with pressure.

The fabrication procedures for the stamps illustrated in Figure 2 use multilevel molding and bonding steps with different layers of PDMS.[48] The bulk of the stamp including the body and the surface that supports the reservoir and microchannel structures result from partially curing PDMS (5:1 monomer:crosslinking agent) against a lithographically patterned template. A thin stainless steel washer laminated against the template provides additional levels of relief in the stamp body (Figure S1a, S2a in the Supporting Information) to configure it for integration with a custom automated transfer printing tool. Circular punches (≈600 μm, diameter) around the perimeter of the stamp serve as interfaces between external gas sources and the microchannels/reservoirs. A thin membrane of partially cured PDMS (20:1 monomer:crosslinking agent) bonds to the molded stamp surface upon thermal curing, to yield structures that can withstand pressures greater than 12.5 psi before rupture.[49]

2.2. Measuring Adhesion of Actuated Stamps

Vertical pull-off forces measured under a variety of reservoir pressures quantify the effect of inflation and deflation on stamp adhesion characteristics.[40] The measurement setup, shown in Figure S2b (see Supporting Information), consists of a precision load cell (GSO-10, Transducer Techniques) supported on a manual tip/tilt platform and attached to automated *x*-, *y*-translational stages. An independent vertical translational stage (Aerotech PRO 165) coupled with a rotation platform is used to contact the stamp with a target substrate (for this work a silicon wafer) connected to the load cell. Studies entail measurements at various controlled velocities, displacements, and alignments. A microscope objective mounted with the vertical stage and attached to its own secondary lateral translation axes provides visual evaluation of stamp contact and retraction events. The experiments involve contact with a clean, untreated piece of a silicon wafer (≈5 mm × 5 mm, attached to the load cell) at a rate of 5 μm/s and translated by 10 μm beyond initial contact to ensure intimate coupling between substrate and stamp. After a relaxation period of 5 seconds, the stamp is retracted at a controlled velocity. From the resulting force-displacement curves recorded by the load cell, the maximum pull-off force

© 2012 WILEY-VCH Verlag GmbH & Co. KGaA, Weinheim

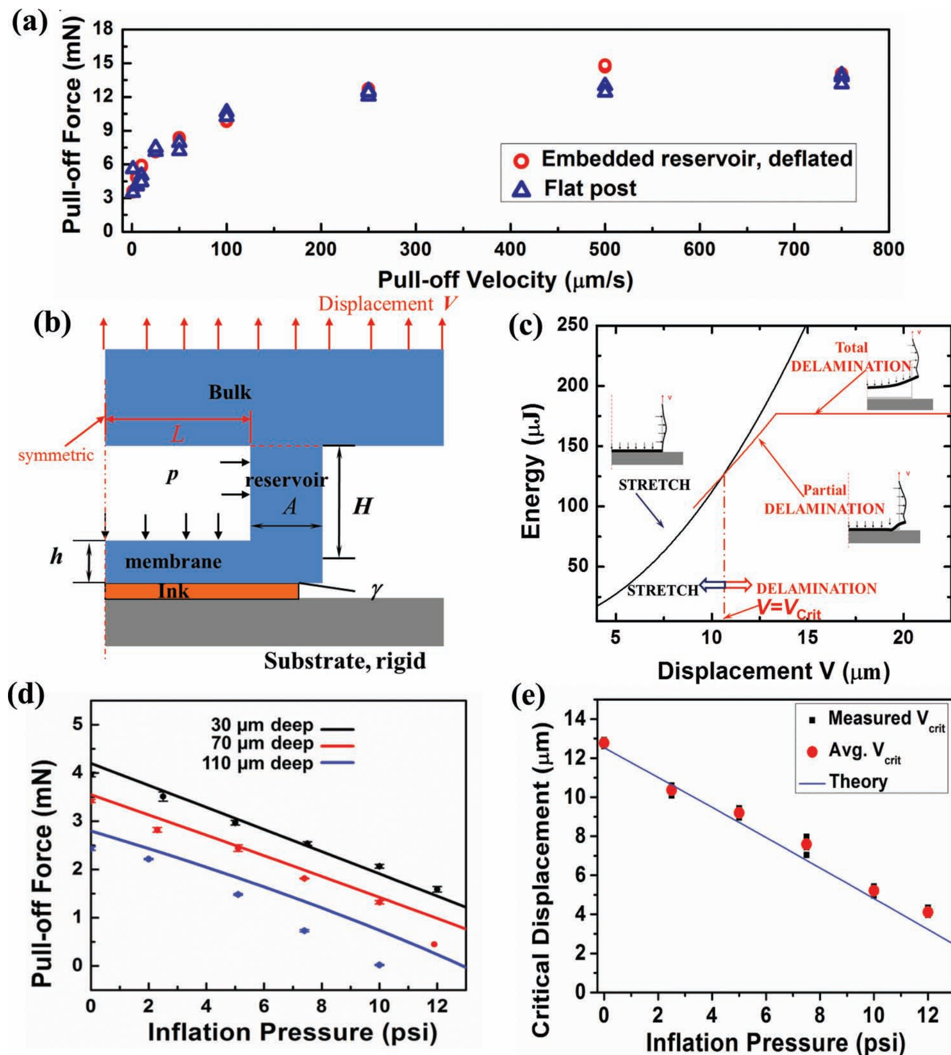

Figure 3. a) Comparison of pull-off forces between stamps having embedded active regions (deflated state) and stamps without reservoir microstructures. b) Schematic cross sectional illustration of an active stamp, with key dimensions, parameters and materials labeled. c) Energy curves for different deformation modes and the critical displacement that separates these modes. d) Experimental and theoretically predicted decrease in stamp/silicon interfacial adhesion (maximum pull-off force) with increasing inflation pressure. e) Experimental and theoretically predicted decrease in critical displacements with increasing inflation pressures.

could be determined for a given delamination speed and reservoir pressure, in a manner similar to that reported previously.[39,40] Effects of inflation on stamp adhesion are evaluated with reserviors pressurized to desired levels while retracting at a fixed velocity. For these studies, after relaxation, retraction of the inflated stamps at 10 μm/s, a velocity consistent with speeds employed in rate-dependent adhesiveless printing, define characteristic pull-off forces.

Representative data for elastomeric stamps with and without embedded reservoirs appear in **Figure 3**. For the case of active stamps, with the membranes deflated, there is a strong velocity dependence in the measured adhesion (Figure 3a).[33,34] The functional dependence, consistent with flat surfaces of similar contact area and having no embedded active regions, arise from the viscoelastic nature of PDMS and demonstrate that the embedded microstructures do not alter significantly the adhesive behavior of the stamp when deflated. Figure 3b,c present schematic details of a mechanics model developed to describe printing from an inflated stamp which is described in the next section. Figure 3d shows a comparison of the measured pull-off forces for reservoirs with depths of 30, 70, and 110 μm at increasing levels of inflation pressure. For the three depths investigated, pull-off forces monotonically decrease with increased inflation, leading to minimum adhesion values between 10 and 12 psi. Reservoirs with depths of 110 μm and pressurized to 10 psi exhibit adhesive forces below the measurement capabilities of the load cell; those with depths of 70 μm approach this limit at pressures in excess of 12 psi. These pull-off forces represent a nearly 50X reduction from the deflated state. Furthermore, by modulating the inflation pressure via electronic switches and gas flow regulators, the pull-off forces can be controllably tuned to specific values through

© 2012 WILEY-VCH Verlag GmbH & Co. KGaA, Weinheim

mechanisms external to the stamp/transfer printing system. This type of active, tunable control of adhesion yields new levels of versatility and operational modes in transfer printing, as demonstrated subsequently.

3. Mechanics Modeling of Active, Inflatable Stamps

An analytical mechanics model was developed to study the printing process. Figure 3b shows all key geometric and material properties of an inflatable stamp, a thin plate of ink, and a receiver substrate. The reservoir and the membrane are modeled as beams (illustrated in insets of Figure 3c) having different elastic constants (E_R, E_M, and μ for the reservoir, membrane moduli, and bulk shear modulus, respectively) corresponding to the different PDMS formulations used to fabricate the stamps. Inflation pressure is treated throughout as a uniform distributed pressure denoted by p. A displacement V applied at the top of the bulk region of the stamp results in a displacement (stretch) V_0 at the top of the reservoir (horizontal dashed line in Figure 3b). The relation between V_0 and V is defined by the equilibrium condition (see Supporting Information for details) as

$$V = V\left[1 + \frac{E_R(L+A)}{4\pi\mu H} g_2\left(\frac{A}{L}\right)\right] - \frac{p(L+A)}{4\pi\mu} g_1\left(\frac{A}{L}\right) \tag{1}$$

where H, A and E_R are the depth, width and Young's modulus of the reservoir (Figure 3b), respectively, L is the half width of the membrane (Figure 3b) and g_1, g_2 are functions obtained analytically in the Supporting Information. For small V (and therefore small V_0), the interfacial adhesion between the ink and the stamp prevents the membrane from delaminating. In this regime, only the reservoir is stretched and bent by the inflation pressure. Our model treats the system as a double clamped beam subjected to pressure p, where the deflection, w_R is given by, $w_R = py^2(y-H)^2/(2E_R A^3)$. The coordinates $y = 0$ and $y = H$ denote the two ends of the reservoir. The potential energy $U_{stretch}$ includes contributions from the membrane and bending energies of the reservoir, and the work done by p, which yields

$$U_{stretch} = \frac{E_R A}{2}\left(\frac{V_0}{H}\right)^2 H + \int_0^H p w_R \, dy = \frac{E_R A V_0^2}{2H} - \frac{p^2 H^5}{120 E_R A^3} \tag{2}$$

As the displacement V_0 increases, the membrane starts to delaminate from the ink. If l denotes the delamination length (starting at the outer perimeter), then the potential energy $U_{delaminate}$ consists of the membrane and bending energies of the reservoir and the bending energy of the membrane, the work done by p, and also the adhesive energy of the interface. Minimization of potential energy, according to the condition $\partial U_{delaminate}/\partial l = 0$ gives the delamination length l and therefore $U_{delaminate}$ as (see Supporting Information for details)

$$U_{delaminate} = \gamma H \cdot f\left(\frac{V_0}{H\sqrt{\frac{\gamma}{E_R A}}}, \frac{pH}{\sqrt{\gamma E_R A}}, \frac{A}{H}, \frac{E_M h^3}{E_R A^3}\right) \tag{3}$$

where E_M and h are the Young's modulus and thickness of the membrane, respectively, and γ is the work of adhesion of the stamp/ink interface and the function f is specified in the Supporting Information. It should be noted that γ (and therefore the pull-off force) depends on the peeling rate due to viscoelastic effects[33,34] as is shown in Figure 3a. The comparison (Figure 3d–f) between the following analysis and the experiments is based on the peeling rate of 10 µm/s while ink delivery which corresponds to $\gamma \approx 0.16$ N/m. Equation (3) holds until the membrane completely delaminates from the ink, i.e., when the delamination length l reaches the half width L of the membrane (Figure 3b), after which $U_{delaminate}$ does not increase with V_0 (or V, as illustrated in Figure 3c).

Figure 3c compares the energies for the two deformation modes in Equations (2) and (3) versus the displacement V at the top of the bulk part of the stamp. (See Equation (1) and Supporting Information for the relationship between V and V_0.) A critical displacement V_{crit} separates the two deformation modes: for $V < V_{crit}$, $U_{stretch}$ is smaller than $U_{delaminate}$ and there is no delamination; for $V > V_{crit}$, delamination is energetically favored. The maximum pulling force is reached when $V = V_{crit}$-0, just prior to delamination. The critical displacement V_{crit} corresponds to a critical value of V_0 which is denoted here as $V_{0\text{-crit}}$. The resulting maximum pulling force is obtained analytically as

$$p_{pull-off} = \frac{4 E_R A V_{0-crit}(L+A)}{H} - p\pi L^2 \tag{4}$$

(see Supporting Information for details of calculations), which agrees well with the experiments (Figure 3d), as does the critical displacement (Figure 3e) under various inflation pressures between 0 ~ 12 psi and for different reservoir depths (see Supporting Information for details). Figure 3b–e suggest that, as the inflation pressure increases, the pull-off force and the critical displacement to delaminate the stamp from the ink decrease, thereby promoting release of inks onto receiver substrates. Similar trends are evident for reservoirs with differing geometries (Figure S3, Supporting Information). These experimentally validated models not only illustrate the key mechanics involved in this class of stamp, but they can also be used to guide advanced designs.

4. Transfer Printing Capabilities Enabled by Active Stamp Designs

4.1. Adhesiveless Printing onto Unusual and Challenging Substrates

Examples of enhanced printing capabilities enabled by the stamps described in previous sections appear in **Figure 4**, in which multiple silicon plates are integrated onto a variety of unusual surfaces not easily accessible through other schemes. Figure 4a presents an optical image of silicon plates (250 µm × 250 µm × 3 µm) arranged in a 3 × 3 array on a bare sheet of polyethylene terephthalate (PET; 50 µm in thickness), bent around a glass cylinder (20 mm radius of curvature) after printing. The inset of Figure 4a shows an angled array of plates as they wrap around the curve of the underlying cylinder. An example of printing of similar structures onto commercially available

 © 2012 WILEY-VCH Verlag GmbH & Co. KGaA, Weinheim

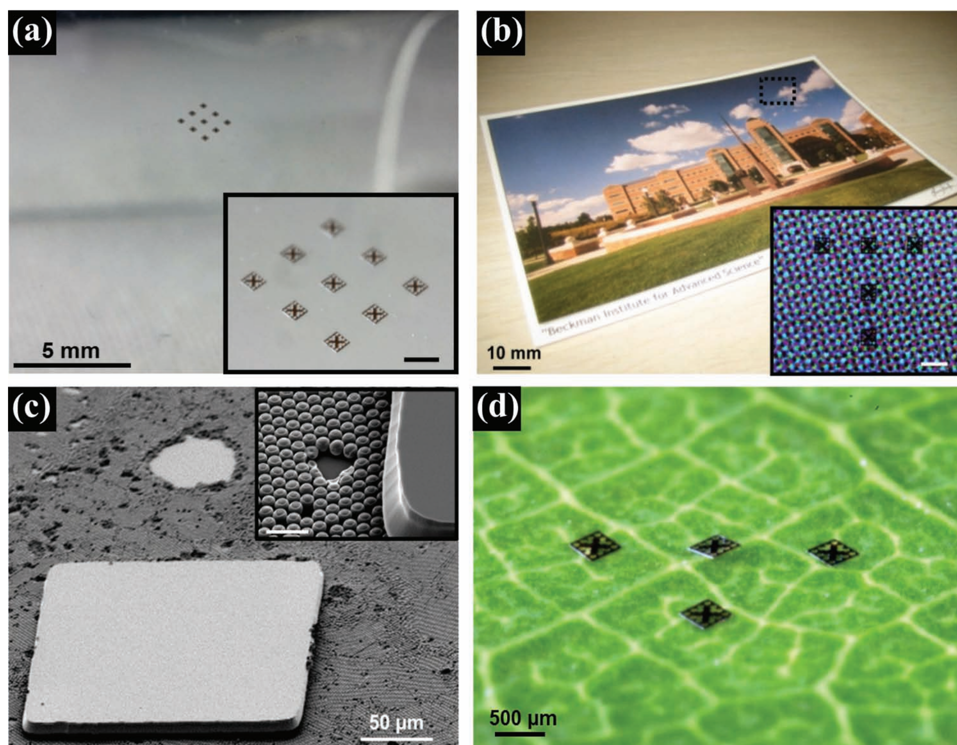

Figure 4. Printing demonstrations achieved with active stamps. Stamps pressurized to 12 psi enabled delivery of silicon plates (250 µm × 250 µm × 3 µm) onto a number of unusual substrates, without the use of adhesive layers, such as a) plastic sheets (PET, 50 µm thick), b) glossy card stock, c) photonic crystals (PC), and d) organic matter such as a leaf. Insets in (a,b) show printed arrays of plates on the respective substrates with scale bars corresponding to 250 µm. Inset in (c) shows the PC surface composed of SiO_2 microspheres, scale bar corresponds to 4 µm.

card stock (smooth, non-matte finish), appears in Figure 4b, and is potentially relevant to paper-based electronics. Printing onto textured surfaces is also possible, as in Figure 4c which shows a SEM micrograph of a silicon plate (200 µm × 200 µm × 3 µm) delivered onto a photonic crystal (PC) surface consisting of close-packed array of SiO_2 microspheres (600 nm in radius). This type of integration could be of interest in unusual opto-electronics systems.[50,51]

Figure 4d provides a similar demonstration of adhesiveless transfer onto a surface with substantial relief, in this case onto the underside of a leaf. As shown in the image, silicon plates are located over the lower cuticle of the leaf as well as the venation and part of the midrib. Due to the coarse and non-planar nature of the venation, the plates are unable to establish complete contact with the cuticle, leaving them propped and partially suspended. Active stamps are particularly effective printing tools in this case due to the ease with which the rigid plates can rotate and deflect along with the thin, soft inflated membrane, allowing them to self-position on the receiver and maintain maximum available contact. Passive stamp designs, such as those that use solid, molded posts, do not offer this type of self-adjustment due to their comparatively high levels of rigidity. The ability to print single crystal silicon structures directly onto naturally occurring, biological surfaces could be of value in the integration of semiconductor device functionality with living systems.[52–56] Further demonstrations of the printing capabilities afforded by active stamp designs are shown in Figure S4, including silicon chips deployed onto textured surfaces of coins and stacked in highly aligned multilayer configurations.

4.2. Programmable, Multireservoir Active Stamps

The stamp and reservoir designs described thus far can be scaled to include multiple embedded features formed in independent and interconnected layouts. **Figure 5**a provides a series of optical images that demonstrate the arrangement and printing of five, independently addressable reservoirs, each with layouts like those in Figure 2. Simultaneous inking of all five active regions occurs by contacting the stamp to an array of silicon plates with separations that match those of the reservoirs. After retrieval, an inked stamp of this type can be positioned over a target substrate (PDMS-coated paper) as shown in panel (*i*). Panels (*ii*) and (*iii*) correspond to actuation of the first, third, and fifth reservoirs and the second and fourth reservoirs, respectively, achieved by activating individual switches connected to gas inlets for each reservoir. To demonstrate independent printing capabilities, panels (*iv*)–(*vi*) show arrangement and delivery of selected silicon plates onto the substrate surface, highlighting the unique assemblies that can be obtained with this multireservoir design. Independent actuation of selected reservoirs out of an array enables rapid deployment of large quantities of inks in a controlled, deterministic manner which is not limited to density, pitch, or layout limitations of the donor material. Figure 5b

© 2012 WILEY-VCH Verlag GmbH & Co. KGaA, Weinheim

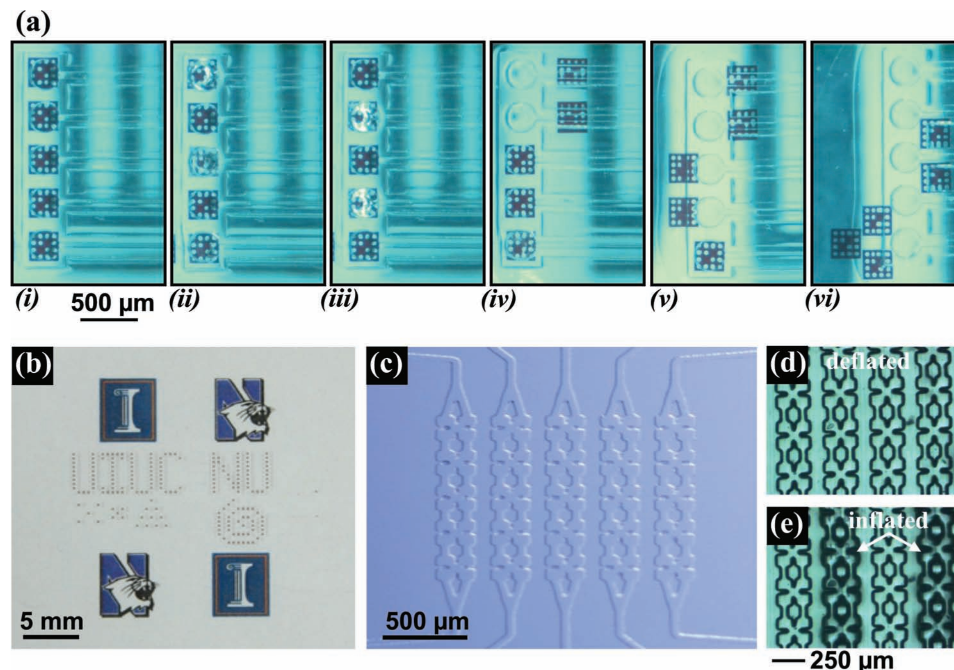

Figure 5. Multiple, independently addressable active stamps configured for programmable printing modalities. a) Series of frames demonstrating actuation and printing of 5 microreservoirs in a single stamp. After retrieval, (*i*), the inked stamp is positioned above a 1 mm thick sheet of PDMS laminated to a business card. (*ii*) and (*iii*) show actuation of the first, third, and fifth reservoir (from the top) and second and fourth reservoir, respectively. After printing the first two plates, (*iv*), the stamp is moved to a different location to print the third and fourth plates, (*v*). Finally the last plate is delivered near the fourth plate, (*vi*), demonstrating the positioning and deployment capabilities of a programmable stamp. b) Silicon plates printed in various geometries on a PDMS sheet laminated against a piece of paper using a stamp similar to the one in (a). Other configurations of programmable stamps are also demonstrated in (c), including series of interconnected reservoirs used to actuate entire columns of a stamp. d) A magnified view of (c) with interlinked reservoirs that can inflate alternating columns when pressurized, (e).

provides an optical image of silicon plates printed in diverse arrangements using the stamp shown in Figure 5a. As demonstrated here, a variety of different layouts can be accommodated with a single stamp, potentially increasing printing throughput with massively parallel assembly strategies.

Multireservoir designs can also be used in ways such that different active regions are coupled with neighboring structures to provide extended regions of inflation for printing large or asymmetric ink structures. Figure 5c shows a (5×5) array of cross-shaped reservoirs connected via microchannels along vertical rows, resulting in long columns that are actuated independently or with other regions of the stamp. Actuating alternating reservoir columns yields responses illustrated in magnified views of Figure 5d,e, respectively, where inflated columns are denoted by dark lines along the perimeters of the reservoirs. To ensure proper inflation over the extended active regions, compressed gas is provided from two inlets on the top and bottom of each column. The large, interconnected layout provides many of the same capabilities as the independently addressable reservoirs, such as pitch control and versatility of ink arrangements, but adds flexibility in the size, type, and configuration of the ink material available for printing.

5. Conclusions

In summary, elastomer structures that embed actuatable, near-surface reservoirs and microchannels allow controllable tuning of the strength and geometry of interfacial adhesion. When used in stamps for transfer printing, selective pressurization of the reservoirs results in localized regions of inflation on the stamp surface, inducing interfacial separation mechanics with a solid ink to enhance printing capabilities. Such designs provide universal, programmable tools for deterministic assembly of classes of materials and substrates that have been previously difficult to address, thereby creating engineering opportunities in areas such as novel forms of electronics and opto-electronics which require intimate contact with substrates in curvilinear formats or unusual environments.

6. Experimental Section

Templates for Stamps: Bare silicon wafers (Montco Silicon) were degreased with acetone, isopropyl alcohol, and deionized water prior to exposure to a UV/ozone environment for 5 min. Spin casting defined a layer of negative tone photoactive epoxy (SU8-50, MicroChem; 70 μm in thickness) that was then baked at 120 °C on a hotplate for 10 min to remove residual solvent. Exposure to UV radiation (185 mJ cm^{-2}, λ = 365 nm) through a quartz mask defined desired patterns, followed by a second annealing step for 10 min on a hotplate at 120 °C. Development produced a structure for direct molding of PDMS. Prior to molding, the surface of the template was treated with (tridecafluoro-1,1,2,2-tetrahydrooctyl) trichlorosilane (FOTCS, United Chemicals) via vapor deposition.

Active Stamps with Embedded Circular Reservoirs: Fabricating stamps with embedded reservoirs and microchannels involved a

© 2012 WILEY-VCH Verlag GmbH & Co. KGaA, Weinheim

series of molding and bonding steps with different layers of PDMS (Figure S1a, Supporting Information). The stamp body with molded surface relief was first generated by pouring a precursor of liquid PDMS (5:1 monomer:crosslinking agent) against a photolithographically patterned template. A thin (≈2.6 mm) washer inserted against the template prior to applying the liquid PDMS created a multilevel stamp with a wide base for integration with a custom automated transfer printing tool. The PDMS was then partially cured in an oven at 70 °C for 20 min, cooled, and demolded from the template and washer. After cooling, circular holes were formed by punching a 20 gauge, blunt-edge syringe needle attached to a manual drill press through the stamp bulk. The punches were positioned so that only microchannels connecting to the active reservoir regions were pierced. The stamps were then cleaned with pressure sensitive tape prior to application of the capping membrane.

The thin surface membrane was formed by spin coating (3000 RPM, 30 s) a PDMS mixture of 20:1 monomer:crosslinking agent onto a silicon wafer treated with FOTCS anti-adhesion layers and partially curing at 70 °C for 11 min on a hotplate. Following the partial cure, the molded 5:1 PDMS was immediately placed onto the warm membrane and the curing finished in an oven at 75 °C for 4 h. When removed from the oven and cooled, the stamp was peeled off the wafer surface intact, with the membrane chemically bonded to the bulk of the stamp.

Active Stamp Imprints and Characterization: Imprints of active stamps with circular reservoirs were obtained under different levels of membrane inflation. Small plastic containers were filled with a low viscosity, photocurable polyurethane (4 cc of NOA 65, Norland Optical Adhesives) and attached to manual *x*-, *y*-stages under a stereoscope. Active stamps on an independent *z*-stage were lowered to bring the inflatable regions into contact with the NOA. After ≈5 min in this position, the stamps were inflated and held in the inflated state for another 5 min to allow the fluid to flow around and conform to the active regions. The entire setup was then exposed to UV light for 60 min to cure the NOA. The reservoirs were deflated, carefully demolded, and cleaned. The imprints were evaluated with a surface profilometer (Dektak 3030). Line scans obtained at the center of the imprint (coinciding with the center of the reservoir) were used to calculate the maximum deflection of the membranes under increasing inflation pressure.

Semiconductor Inks: Figure S1b (Supporting Information) shows the procedures used to create silicon plates.[57] These plates were derived from silicon-on-insulator (SOI) wafers with 3 μm thick device layers (top silicon), 1.1 μm thick buried oxide layers (BOx) and 450 μm thick handle substrates (supporting wafer). Plates with lateral dimensions ranging from 200 μm to 250 μm were defined by a layer of photoresist (AZ 5214E, AZ Electronic Materials) that served as a resist for reactive ion etching (RIE, PlasmaTherm RIE) of the top silicon. Bathing the chip in concentrated hydrofluoric acid (HF, 49%) for 55 s removed the exposed BOx and partially undercut the silicon plates, resulting in a narrow (≈1.1 μm) trenches along the their perimeters. The substrate was then cleaned in Piranha solution (3:1 sulfuric acid:hydrogen peroxide) for 3 min, rinsed, and coated with a 1.5 μm layer of photoresist (AZ 5214E). Flood exposing the photoresist in a mask aligner (Karl Suss MJB3) with UV radiation (150 mJ cm^{-2}), exposed all of the photoresist except in the partially undercut regions along the plates. Developing for 45 s in basic solution (AZ Electronic Materials, MIF 327) removed the exposed photoresist. The plates were then undercut etched in concentrated HF for 4.5 h to remove the remaining BOx. These procedures left the plates tethered to the handle by the narrow rim of photoresist that remained along their perimeters.

Transfer Printing: Precision translation and rotational stages controlled the positions of stamp, ink, and receiver substrates during the various printing steps illustrated in Figure 1. An optical microscope and video acquisition system enabled visual monitoring of the process while an external gas source delivered compressed nitrogen for local inflation of the microreservoirs and channels. The stages also accommodated a custom adhesion measurement system designed to measure pull-off forces of stamp under various amounts of inflation shown in Figure S2b (Supporting Information).

Supporting Information

Supporting Information is available from the Wiley Online Library or from the author.

Acknowledgements

A.C. and S.W contributed equally to this work. General characterization and processing facilities were provided through the Frederick Seitz Materials Research Laboratory (MRL) with support from the University of Illinois and from DoE grants DE-FG02-07ER46453 and DE-FG02-07ER46471. For the silicon printing demonstrations, the authors acknowledge support from a MURI award on silicon nanomembranes, award FA9550-08-1-0394. For adhesion measurement systems and automated printers, the authors acknowledge the center for Nanoscale Chemical Electrical Mechanical Manufacturing Systems in University of Illinois, which is funded by National Science Foundation under grant CMMI-0328162. The authors thank B. Sankaran for assistance with processing at MRL and C. Bee and S. Robinson for assistance with imaging at Beckman Institute for Advanced Science and Technology. A.C. acknowledges support from the Department of Defense (DoD) through the National Defense Science and Engineering Graduate (NDSEG) Fellowship program.

Received: April 12, 2012
Published online: June 20, 2012

[1] J.-H. Ahn, H.-S. Kim, K. J. Lee, S. Jeon, S. J. Kang, Y. Sun, R. G. Nuzzo, J. A. Rogers, *Science* **2006**, *314*, 1754.
[2] J. Yoon, A. J. Baca, S.-I. Park, P. Elvikis, J. B. G. III, L. Li, R. H. Kim, J. Xiao, S. Wang, T.-H. Kim, M. J. Motala, B. Y. Ahn, E. B. Duoss, J. A. Lewis, R. G. Nuzzo, P. M. Ferreira, Y. Huang, A. Rockett, J. A. Rogers, *Nat. Mater.* **2008**, *7*, 907.
[3] J. Yoon, S. Jo, I. S. Chun, I. Jung, H.-S. Kim, M. Meitl, E. Menard, X. Li, J. J. Coleman, U. Paik, J. A. Rogers, *Nature* **2010**, *465*, 329.
[4] A. Javey, S. Nam, R. S. Friedman, H. Yan, C. M. Lieber, *Nano Lett.* **2007**, *7*, 773.
[5] K. Takei, T. Takahashi, J. C. Ho, H. Ko, A. G. Gillies, P. W. Leu, R. S. Fearing, A. Javey, *Nat. Mater.* **2010**, *9*, 821.
[6] D. R. Hines, A. E. Southard, A. Tunnell, V. Sangwan, T. Moore, J.-H. Chen, M. S. Fuhrer, E. D. Williams, *Proc. SPIE* **2007**, *6658*, 66580Y.
[7] Q. Cao, J. A. Rogers, *Adv. Mater.* **2009**, *21*, 29.
[8] Y. Lee, S. Bae, H. Jang, S. Jang, S.-E. Zhu, S. H. Sim, Y. I. Song, B. H. Hong, J.-H. Ahn, *Nano Lett.* **2010**, *10*, 490.
[9] Q. Guo, X. Teng, S. Rahman, H. Yang, *J. Am. Chem. Soc.* **2003**, *125*, 630.
[10] Q. Guo, X. Teng, H. Yang, *Adv. Mater.* **2004**, *16*, 1337.
[11] Y.-L. Loo, D. V. Lang, J. A. Rogers, J. W. P. Hsu, *Nano Lett.* **2003**, *3*, 913.
[12] S. W. Nam, X. Jiang, Q. Xiong, D. Ham, C. Lieber, *Proc. Natl. Acad. Sci. USA* **2009**, *106*, 21035.
[13] J. Xiang, W. Lu, Y. Hu, Y. Wu, H. Yan, C. Lieber, *Nature* **2006**, *441*, 489.
[14] G. Yu, C. M. Lieber, *Pure Appl. Chem.* **2010**, *82*, 2295.
[15] A. J. Tunnell, V. W. Ballarotto, D. R. Hines, E. D. Williams, *Appl. Phys. Lett.* **2008**, *93*, 193113.
[16] X. Liang, Z. Fu, S. Y. Chou, *Nano Lett.* **2007**, *7*, 3840.
[17] H. C. Ko, A. J. Baca, J. A. Rogers, *Nano Lett.* **2006**, *6*, 2318.
[18] A. J. Baca, M. A. Meitl, H. C. Ko, S. Mack, H.-S. Kim, J. Dong, P. M. Ferreira, J. A. Rogers, *Adv. Funct. Mater.* **2007**, *17*, 3051.
[19] A. J. Baca, J.-H. Ahn, Y. Sun, M. A. Meitl, E. Menard, H.-S. Kim, W. M. Choi, D.-H. Kim, Y. Huang, J. A. Rogers, *Angew. Chem. Int. Ed.* **2008**, *47*, 5524.

© 2012 WILEY-VCH Verlag GmbH & Co. KGaA, Weinheim

[20] A. C. Ford, J. C. Ho, Z. Fan, O. Ergen, V. Altoe, S. Aloni, H. Razavi, A. Javey, *Nano Res.* **2008**, *1*, 32.
[21] J. Yeom, M. A. Shannon, *Adv. Funct. Mater.* **2010**, *20*, 289.
[22] Y. Xia, G. M. Whitesides, *Angew. Chem. Int. Ed.* **1998**, *37*, 551.
[23] J. L. Wilbur, A. Kumar, H. A. Biebuyck, E. Kim, G. M. Whitesides, *Nanotechnology* **1996**, *7*, 452.
[24] Z. Bao, J. A. Rogers, H. E. Katz, *J. Mater. Chem.* **1999**, *9*, 1895.
[25] A. L. Briseno, M. Roberts, M.-M. Ling, H. Moon, E. J. Nemanick, Z. Bao, *J. Am. Chem. Soc.* **2006**, *128*, 3880.
[26] G. B. Blanchet, Y.-L. Loo, J. A. Rogers, F. Gao, C. R. Fincher, *Appl. Phys. Lett.* **2003**, *82*, 463.
[27] M. M. Stevens, M. Mayer, D. G. Anderson, D. B. Weibel, G. M. Whitesides, R. Langer, *Biomaterials* **2005**, *26*, 7636.
[28] M. Xue, Y. Yang, T. Cao, *Adv. Mater.* **2008**, *20*, 596.
[29] Y.-L. Loo, R. L. Willett, K. W. Baldwin, J. A. Rogers, *Appl. Phys. Lett.* **2002**, *81*, 562.
[30] E. Menard, K. J. Lee, D.-Y. Khang, R. G. Nuzzo, J. A. Rogers, *Appl. Phys. Lett.* **2004**, *84*, 5398.
[31] E. Menard, M. A. Meitl, Y. Sun, J.-U. Park, D. J. Shir, Y.-S. Nam, S. Jeon, J. A. Rogers, *Chem. Rev.* **2007**, *107*, 1117.
[32] Y. Sun, H.-S. Kim, E. Menard, S. Kim, I. Adesida, J. A. Rogers, *Small* **2006**, *2*, 1330.
[33] M. A. Meitl, Z.-T. Zhu, V. Kumar, K. J. Lee, X. Feng, Y. Y. Huang, I. Adesida, R. G. Nuzzo, J. A. Rogers, *Nat. Mater.* **2006**, *5*, 33.
[34] X. Feng, M. A. Meitl, A. M. Bowen, Y. Huang, R. G. Nuzzo, J. A. Rogers, *Langmuir* **2007**, *23*, 12555.
[35] Z. Qiang, H. Yang, L. Chen, H. Pang, Z. Ma, W. Zhou, *Appl. Phys. Lett.* **2008**, *93*, 061106.
[36] H. Kim, E. Brueckner, J. Song, Y. Li, S. Kim, C. Lu, J. sulking, K. Choquette, Y. Huang, R. G. Nuzzo, J. A. Rogers, *Proc. Natl. Acad. Sci. USA* **2011**, *108*, 10072.
[37] S.-I. Park, Y. Xiong, R.-H. Kim, P. Elvikis, M. Meitl, D.-H. Kim, J. Wu, J. Yoon, C.-J. Yu, Z. Liu, Y. Huang, K.-C. Hwang, P. Ferreira, X. Li, K. Choquette, J. A. Rogers, *Science* **2009**, *325*, 977.
[38] S. A. Fortuna, J. Wen, I. S. Chun, X. Li, *Nano Lett.* **2008**, *8*, 4421.
[39] A. Carlson, H.-J. Kim-Lee, J. Wu, P. Elvikis, H. Cheng, A. Kovalsky, S. Elgan, Q. Yu, P. M. Ferreira, Y. Huang, K. T. Turner, J. A. Rogers, *Appl. Phys. Lett.* **2011**, *98*, 264104.
[40] S. Kim, J. Wu, A. Carlson, S. H. Jin, A. Kovalsky, P. Glass, Z. Liu, N. Ahmed, S. L. Elgan, W. Chen, P. M. Ferreira, M. Sitti, Y. Huang, J. A. Rogers, *Proc. Natl. Acad. Sci. USA* **2010**, *107*, 17095.
[41] A. D. Lees, J. Hardie, *J. Exp. Biol.* **1987**, 209.
[42] T.-H. Kim, A. Carlson, J.-H. Ahn, S. M. Won, S. Wang, Y. Huang, J. A. Rogers, *Appl. Phys. Lett.* **2009**, *94*, 113502.
[43] P. Kim, K. W. Kwon, M. C. Park, S. H. Lee, S. M. Kim, K. Y. Suh, *Biochip J.* **2008**, *2*, 1.
[44] D. C. Duffy, J. C. McDonald, O. J. A. Schueller, G. M. Whitesides, *Anal. Chem.* **1998**, *70*, 4974.
[45] J. C. McDonald, D. C. Duffy, J. R. Anderson, D. T. Chiu, H. Wu, O. J. A. Schueller, G. M. Whitesides, *Electrophoresis* **1999**, *21*, 27.
[46] J. C. McDonald, G. M. Whitesides, *Acc. Chem. Res.* **2002**, *35*, 491.
[47] F. Wu, L. Li, Z. Xu, S. Tan, Z. Zhang, *Chem. Eng. J.* **2006**, *117*, 51.
[48] M. A. Unger, H.-P. Chou, T. Thorsen, A. Scherer, S. R. Quake, *Science* **2000**, *288*, 113.
[49] M. A. Eddings, J. A. Johnson, B. K. Gale, *J. Micromech. Microeng.* **2008**, *18*, 1.
[50] S. Kim, Y. Su, A. Mihi, S. Lee, Z. Liu, T. K. Bhandakkar, J. Wu, J. B. G. III, H. T. Johnson, Y. Zhang, J.-K. Park, P. V. Braun, Y. Huang, J. A. Rogers, *Small* **2011**, 1.
[51] A. Mihi, C. Zhang, P. V. Braun, *Angew. Chem. Int. Ed.* **2011**, *50*, 5712.
[52] J. Viventi, D.-H. Kim, J. D. Moss, Y.-S. Kim, J. A. Blanco, N. Annetta, A. Hicks, J. Xiao, Y. Huang, D. J. Callans, J. A. Rogers, B. Litt, *Sci. Transl. Med.* **2010**, *2*, 24ra22.
[53] D.-H. Kim, N. Lu, R. Ghaffari, Y.-S. Kim, S. P. Lee, L. Xu, J. Wu, R.-H. Kim, J. Song, Z. liu, J. Viventi, B. d. Graff, B. Elolampi, M. Mansour, M. J. Slepian, S. Hwang, J. D. Moss, S.-M. Won, Y. Huang, B. Litt, J. A. Rogers, *Nat. Mater.* **2011**, *10*, 316.
[54] J. Viventi, D.-H. Kim, L. Vigeland, E. S. Frechette, J. A. Blanco, Y.-S. Kim, A. E. Avrin, V. R. Tiruvadi, S.-W. Hwang, A. C. Vanleer, D. F. Wulsin, K. Davis, C. E. Gelber, L. Palmer, J. V. d. Spiegel, J. Wu, J. Xiao, Y. Huang, D. Contreras, J. A. Rogers, B. Litt, *Nat. Neurosci.* **2011**, *14*, 1599.
[55] D.-H. Kim, J. Viventi, J. J. Amsden, J. Xiao, L. Vigeland, Y.-S. Kim, J. A. Blanco, B. Panilaitis, E. S. Frechette, D. Contreras, D. L. Kaplan, F. G. Omenetto, Y. Huang, K.-C. Hwang, M. R. Zakin, B. Litt, J. A. Rogers, *Nat. Mater.* **2010**, *9*, 511.
[56] D.-H. Kim, N. Lu, R. Ma, Y.-S. Kim, R.-H. Kim, S. Wang, J. Wu, S. M. Won, H. Tao, A. Islam, K. J. Yu, T.-I. Kim, R. Chowdhury, M. Ying, L. Xu, M. Li, H.-J. Chung, H. Keum, M. McCormick, P. Liu, Y.-W. Zhang, F. G. Omenetto, Y. Huang, T. Coleman, J. A. Rogers, *Science* **2011**, *333*, 838.
[57] Y. Yang, Y. Hwang, H. A. Cho, J.-H. Song, S.-J. Park, J. A. Rogers, H. C. Ko, *Small* **2011**, *7*, 484.

© 2012 WILEY-VCH Verlag GmbH & Co. KGaA, Weinheim